The magnetic and metallic degenerate G77-50

J. Farihi,[1]⋆ P. Dufour,[2] R. Napiwotzki[3] and D. Koester[4]

[1]*Department of Physics & Astronomy, University of Leicester, Leicester LE1 7RH*
[2]*Département de Physique, Université de Montréal, Montréal, QC H3C 3J7, Canada*
[3]*Centre for Astrophysics Research, University of Hertfordshire, Hatfield AL10 9AB*
[4]*Institut für Theoretische Physik und Astrophysik, University of Kiel, 24098 Kiel, Germany*

ABSTRACT

An accumulation of multi-epoch, high-resolution optical spectra reveal that the nearby star G77-50 is a very cool DAZ white dwarf externally polluted by Mg, Fe, Al, Ca and possibly Na, Cr, Mn. The metallic and hydrogen absorption features all exhibit multiple components consistent with Zeeman splitting in a $B \approx 120$ kG magnetic field. Ultraviolet through infrared photometry combined with trigonometric parallaxes yield $T_{\rm eff} = 5310$ K, $M = 0.60$ M$_\odot$ and a cooling age of 5.2 Gyr. The space velocity of the white dwarf suggests possible membership in the Galactic thick disc, consistent with an estimated total age of 8.6 Gyr. G77-50 is spectrally similar to G165-7 and LHS 2534; these three cool white dwarfs comprise a small group exhibiting both metals and magnetism.

The photospheric metals indicate accretion of rocky debris similar to that contained in asteroids, but the cooling age implies that a remnant planetary system should be stable. A possibility for G77-50 and similarly old, polluted white dwarfs is a recent stellar encounter that dynamically rejuvenated the system from the outside-in. Metal abundance measurements for these cooler white dwarfs have the potential to distinguish material originating in outer region planetesimals injected via fly-by. If common envelope evolution can generate magnetic fields in white dwarfs, then G77-50 and its classmates may have cannibalized an inner giant planet during prior evolution, with their metals originating in terrestrial bodies formed further out. Although speculative, this scenario can be ruled out if terrestrial planet formation is prohibited in systems where a giant planet has migrated to the inner region nominally engulfed during the post-main sequence.

Key words: stars: abundances – circumstellar matter – stars: evolution – stars: magnetic field – planetary systems – white dwarfs.

1 INTRODUCTION

Metal-enriched white dwarfs have experienced a resurgence of interest coinciding roughly with the launch of *Spitzer*. Beginning with the landmark study of Zuckerman et al. (2003), evidence has gradually accumulated supporting a picture whereby most, if not all cool, metal-lined white dwarfs obtain their photospheric heavy elements via rocky bodies similar in composition and in mass to large Solar system asteroids (Jura 2006; Farihi et al. 2010b). Data substantiating this picture comes primarily from *Spitzer* photometric detections of infrared excess indicating circumstellar dust orbiting within the Roche limit of a substantial fraction of metal-contaminated white dwarfs (von Hippel et al. 2007; Farihi, Jura & Zuckerman 2009), and via mid-infrared spectroscopy of the disc material, revealing silicate minerals (primarily olivines) associated with rocky planet formation (Reach et al. 2005; Jura, Farihi & Zuckerman 2009a).

A powerful example of the scientific potential inherent in these stars is the spectacularly polluted white dwarf GD 362 (Gianninas, Dufour & Bergeron 2004; Kawka & Vennes 2005). This system shows remarkable infrared excess emission from closely orbiting dust, reprocessing over 3 per cent of the incident stellar flux and exhibiting perhaps the strongest silicate emission feature associated with *any* mature star (Jura et al. 2007). The optical spectrum of GD 362 displays 15 elements heavier than helium in an abundance pattern mimicking the Earth–Moon system (Zuckerman et al. 2007). The convection zone of the star has been enriched, at a bare minimum, by the equivalent of a 240-km asteroid, and possibly by a body as massive as Callisto or Mars, with promising evidence for internal water (Jura et al. 2009b). Thus, white dwarfs enable unique insights into terrestrial planet formation around intermediate-mass stars by providing data that can be obtained in no other way: a lower mass

⋆E-mail: jf123@star.le.ac.uk

limit to, and the bulk chemical composition of, extrasolar rocky, minor or possibly major planets.

This paper investigates the spectral, kinematical and atmospheric properties of the white dwarf WD 0322−019 (G77-50). The star has been known as a very cool and metal-lined degenerate for over 35 yr (Hintzen & Strittmatter 1974), but was only recently found to exhibit split Ca II H and K absorption lines under high-resolution spectroscopy (Zuckerman et al. 2003). Despite similar, high-resolution spectroscopic observations of several hundred white dwarfs (Voss et al. 2007; Koester et al. 2009), including the detection of a few dozen with Ca II K absorption features (Zuckerman et al. 2003; Koester et al. 2005), only G77-50 and possibly LTT 8381 display evidence for Zeeman-split metallic lines. The observational programme and scientific motivation are described in Section 2, while the spectroscopic analysis, photospheric abundances and stellar properties are derived in Section 3. The discussion of the results is contained in Section 4, where potential origins for the metals and magnetism in G77-50 and related objects are explored in some detail.

2 OBSERVATIONS AND DATA

2.1 Echelle spectroscopy

G77-50 was observed a total of 24 times between 2008 October 4 and November 25 at Cerro Paranal with the 8.2-m Very Large Telescope Unit 2 using the Ultraviolet and Visual Echelle Spectrograph (UVES; Dekker et al. 2000). Spectroscopy was performed over the two detectors covering wavelengths from 3200 to 6650 Å using a standard dichroic configuration with $\lambda_c = 3900/5640$ Å, resulting in two narrow gaps in spectral coverage near 4550 and 5650 Å. A slitwidth of 1.0 arcsec was employed with 2×2 binning, resulting in a nominal resolving power of $R \approx 40\,000$ in both the UV–Blue and Red arms of the instrument. The observations were taken at random intervals that were broadly logarithmic in temporal spacing, with each data set consisting of two consecutive 900-s exposures. The featureless white dwarf WD 0000−345 (LHS 1008) was observed as a spectral standard on 2008 October 8 using an identical instrumental set-up.

The echelle data were processed with the UVES pipeline version 4.3.0, including cosmic ray masking, flat fielding, wavelength calibration, order merging and distilled using optimal aperture extraction. Raw spectra produced in this manner had signal-to-noise (S/N) ratios that fell between 16 and 22 at 5000 Å. The spectral standard data were interpolated in wavelength to match the solution for the science target and smoothed by 121 pixels (3.5–4.0 Å). The science target was divided by the spectral standard and the resulting spectrum was multiplied by an appropriate temperature blackbody to achieve a relative flux calibration.

The 2008 UVES data set was supplemented by two archival UVES observations of G77-50 taken for the SPY survey in 2000 (Napiwotzki et al. 2003), and fully reduced Keck HIRES spectra obtained in 1999 and 1998 (Zuckerman et al. 2003). After correcting for heliocentric velocity at the time of individual exposures, a master spectrum was constructed from the normalized co-addition of all 26 UVES spectra. The resulting spectrum has a binwidth of 0.1 Å, which increases the S/N, while reducing the original resolution to approximately match the decrease resulting from the wavelength shifts observed in the Ca II H and K lines (see Section 3). This spectrum is displayed in Fig. 1, while Table 1 lists prominent stellar features and non-stellar artefacts.

3 SPECTROSCOPIC ANALYSIS AND SYSTEM PARAMETERS

G77-50 is listed as a binary suspect in Bergeron, Ruiz & Leggett (1997) based on the shape of its Hα absorption feature and the lack of a trigonometric parallax distance at that time. Seeming to confirm this hypothesis, Zuckerman et al. (2003) reported the white dwarf as a binary based on what appeared to be double lines of Ca II H and K with large velocity separations, and possible changes in these velocities between two epochs of observation. On the basis of this sound interpretation, the original aim of the UVES programme reported here was to obtain the orbital period and mass ratio of the putative binary by measuring and monitoring the velocities of the Ca II H and K line components. A typical, individual UVES spectrum of G77-50 is shown in the top panel of Fig. 2; it reveals the seemingly double Ca II features first detected by Zuckerman et al. (2003).

3.1 Analysis and interpretation of the 'double' calcium lines

3.1.1 Morphological origins and issues

Initially, the two components seen in the Ca II H and K lines of each UVES spectrum were treated as originating in distinct stellar constituents in a spatially unresolved binary. New measurements taken in 2008 (MJD > 54000) were combined with velocities obtained via identical analysis of archival UVES and Keck HIRES data to determine an orbital period. Each major component of the Ca II features was simultaneously fitted by a Gaussian plus a Lorentzian line profile with the program FITSB2 (Napiwotzki et al. 2004). The parameters of the line profiles were determined simultaneously for all spectra, i.e. assuming a constant line strength and shape (more on this below). The component velocities thus obtained are listed in Table 2. If the measured variations in the line shifts were due to binarity, then each stellar component should exhibit both red and blueshifted lines over time. Under this assumption, a sinusoidal period of almost exactly 2.0 d can be found within the line velocity data.

However, if the observed changes in the Ca II H and K line components are the result of orbital motion in two components of a binary, then the resulting velocity amplitudes predict an essentially equal mass system. One can then estimate the radii and masses of the components based on two independent trigonometric parallaxes for G77-50; Smart et al. (2003) report $\pi = 59.5 \pm 3.2$ mas or $d = 16.8^{+1.0}_{-0.9}$ pc, while the US Naval Observatory (H. Harris, private communication) measure $\pi = 58.02 \pm 0.44$ mas or $d = 17.2^{+0.2}_{-0.1}$ pc. Taking the latter value for the reason of its smaller error, the predicted absolute magnitude of each equally luminous component would be $M_V = 15.7$ mag. At a nominal effective temperature of 5200 K (Bergeron et al. 1997), this corresponds to 0.9 $M_{\odot}$ components.

While this possibility is exciting as the total mass would then easily exceed the Chandrasekhar limit, it also leads to a major inconsistency. The ultraviolet through infrared photometric energy distribution of G77-50 is consistent with a single effective temperature (Fig. 3), and thus if the system were binary, the stars would be twins to all limits of observation, in temperature, in mass-radius and also in metal abundance as the Ca II H and K line components are equally strong. However, the profiles of the Hα line in individual UVES spectra are found to be inconsistent with hydrogen-rich white dwarf models with $\log g > 8.1$; high surface gravities fail to reproduce the observed line. The results of the Hα line fitting are consistent with a single, cool white dwarf at $d = 17.2$ pc as determined by trigonometric parallax.
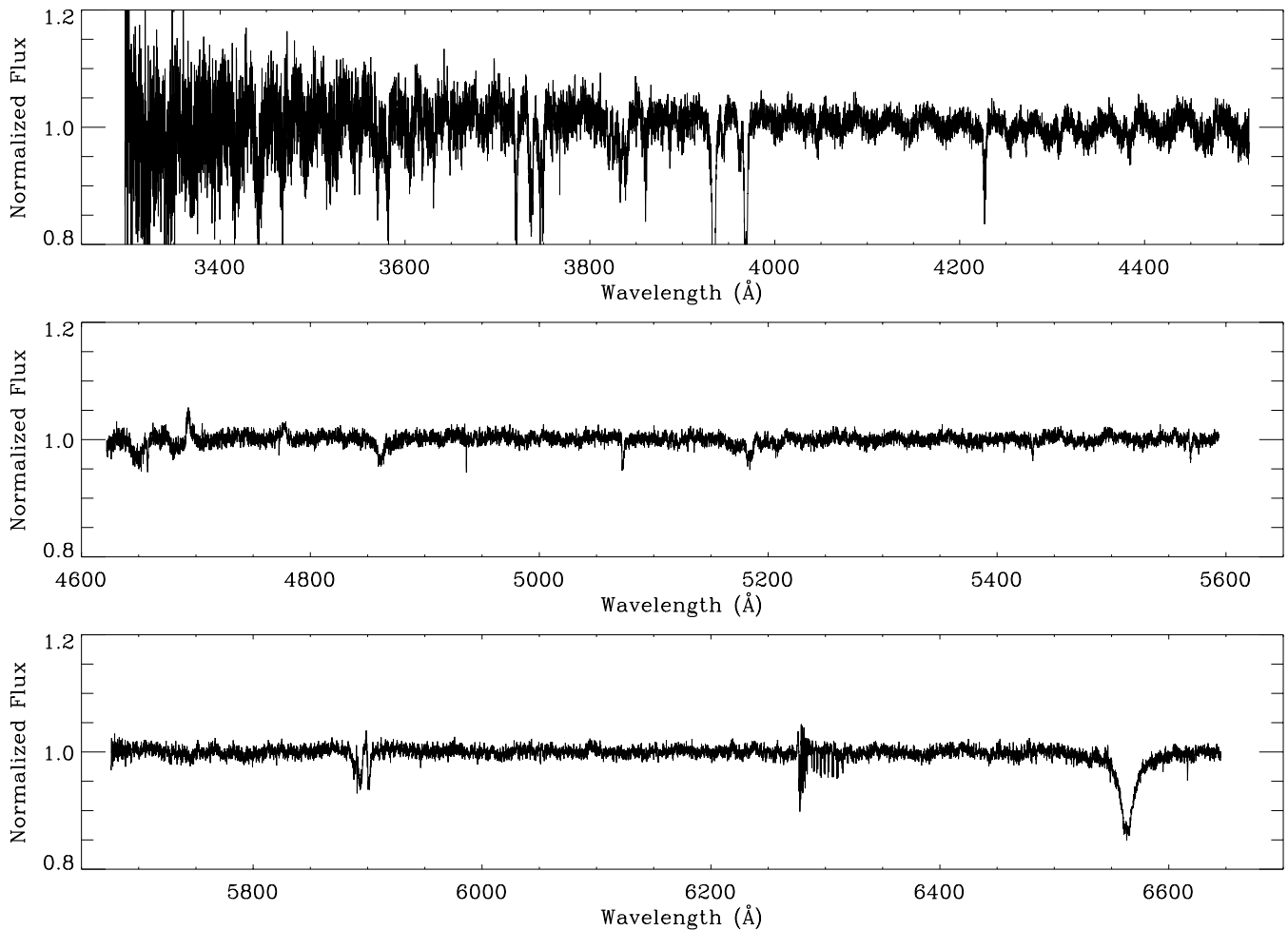
Figure 1. The normalized and co-added UVES spectrum of G77-50, rebinned on to a grid with the spacing of 0.1 Å. The quasi-periodic pattern prominent at shorter wavelengths is due to a light path difference between the flat-field lamp and the sky; this interference is not fully correctable, especially at high S/N. Several previously unidentified metal absorption features are evident, including lines of Mg, Fe, Al, Ca and perhaps Na, Cr, Mn. Hβ is detected for the first time in a very cool white dwarf. There are a large number of weak lines present in the spectrum whose authenticity is uncertain. The features in the green arm below 4700 Å and those in the red arm near 5900 and 6250 Å are detector artefact and telluric absorption residuals (Table 1).

Based on the discrepancies described above, the master spectrum was constructed as detailed in Section 2 and carefully examined by eye. The individual spectra exhibit only Hα, Ca II H and K prominently, but the combination of all UVES exposures yields an S/N $\approx$ 100 spectrum with many additional metal features and weak Hβ absorption. Importantly, all detected features in the co-added spectrum show evidence for multiple components, indicating the presence of a weak magnetic field.

Given the spread in line component velocities as shown in Table 2, it is possible that the lines will be smeared or otherwise diluted by the co-addition of all individual UVES spectra. To investigate the magnitude of this effect, the distribution of line velocities was searched for subgroups with similar values, whose co-addition might result in a better line sensitivity. Two groupings were identified and these spectral subsets were co-added as above: seven spectra with V_+ in the range of 75.5–84.5 km s^{-1} and 15 spectra with V_+ in the range of 87.5–95.5 km s^{-1}. A section of these two spectra are shown in the lower panel of Fig. 2 along with the master spectrum. The noise level of the subset spectra is increased compared to the master data set, and there is no significant change in the shape or depth of the Ca II H and K lines, nor the weak Al I lines. [It is noteworthy that the moderately strong Ca I line shown in the lower-right panel of

Fig. 4 compares favourably in sharpness to both the non-magnetic and the Zeeman-split models (Section 3.2).]

3.1.2 Constraints on line variability and rotation

In this alternative picture, the velocity variation observed in the Ca II H and K line components is most likely due to stellar rotation. Assuming that the star is not seen pole-on, the line-of-sight changes resulting from rotation span a (narrow) range of surface magnetic field strengths, and these induce changes in the strength of the observed Zeeman splitting.

In order to search for periodicities in the wavelength shifts seen in the split H and K lines, a periodogram analysis was performed for (1) $\Delta V = |V_+ - V_-|$ and (2) V_+ and V_- independently. The first approach is adopted here, but the second yielded very similar results. A best fit is found for $P = 29.84579$ d and $\chi^2 = 25.9$, down from 280.5 when assuming constant line velocities, and thus indicating a high statistical significance of the variable solution. The phase-folded velocity differences confirm a good-quality fit with $\chi^2_{\rm red} = 1.04$, with a number of somewhat poorer fits present in the period range of 28–33 d. Two distinct solutions cannot be

Table 1. Notable features in the co-added UVES spectrum of G77−50.

Wavelength (Å)	Absorbing element	Wavelength (Å)	Absorbing element
3441	Fe I	3934	Ca II
3570	Fe I	3944	Al I
3582	Fe I	3962	Al I
3619	Fe I	3968	Ca II
3631	Fe I	4227	Ca I
3648	Fe I	4600−4700	. . .
3720	Fe I	4775	. . .
3735	Fe I	4861	H I
3749	Fe I	5073	. . .
3758	Fe I	5183	Mg I
3767	Fe I	5890	Na I
3820	Fe I	5900	. . .
3832	Mg I	6250−6350	. . .
3838	Mg I	6563	H I
3860	Fe I		

Note. Owing to magnetism, the line centres cannot be determined accurately and the wavelengths given are approximate or laboratory values. In some regions, many lines of Fe I contribute to a single, complex feature but only one wavelength is listed for simplicity. Those features without a corresponding element are due (in part or in whole) to detector artefacts or telluric absorption residuals.

ruled out completely: 1.0311 d ($\chi^2 = 33.8$) and 0.011 333 d ($\chi^2 = 35.6$). The latter period is suspect as it is similar to the length of the individual UVES exposures, while periods near 1.0 d are always dubious, and hence 29.85 d is the most likely solution. For a dipolar field configuration, half a rotation will produce a full cycle in the line velocities; if the long period solution is real, the white dwarf would be a slow rotator.

The relatively strong Ca II features were examined for variation in strength over time within the UVES data set. Measuring reliable equivalent widths for these blended lines was not possible, but the area swept out beneath the continuum was examined as a proxy. Roughly half the feature strengths for both the H and K lines are found in a single, 0.5σ-width peak, with all other measurements sitting below this peak, including some negative (i.e. unphysical) values. Based on this analysis, the individual spectra do not have sufficient S/N to meaningfully constrain variability in the observed line strengths.

3.2 Stellar parameters and abundances

When first studied, Hα was not detected in the optical spectrum of G77−50 and the white dwarf was typed as DG in the classification scheme of the period (Hintzen & Strittmatter 1974). Subsequently, Greenstein (1986) detected Hα and Sion, Kenyon & Aannestad (1990) typed the star in the modern spectral classification as a DZA white dwarf; strongest lines are metallic, weaker line(s) of hydrogen. It is not clear whether feature strength should be determined by depth or equivalent width (E. M. Sion, private communication), but in the case of G77−50, a DAZ classification is readily arguable as its atmosphere is hydrogen rich, with trace metals.

As a first step, T_{eff} and $\log g$ are obtained by refitting existing *BVRIJHK* photometric data with the latest pure hydrogen model atmosphere grid and using the new parallax measurement, following the method of Bergeron et al. (1997). From this, an effective temperature of 5310 ± 100 K and a surface gravity of $\log g = 8.05 \pm 0.01$ are obtained, corresponding to 0.60 ± 0.01 M$_\odot$ and a cooling age of 5.2 ± 0.1 Gyr. Fig. 3 plots the global energy distribution ob-
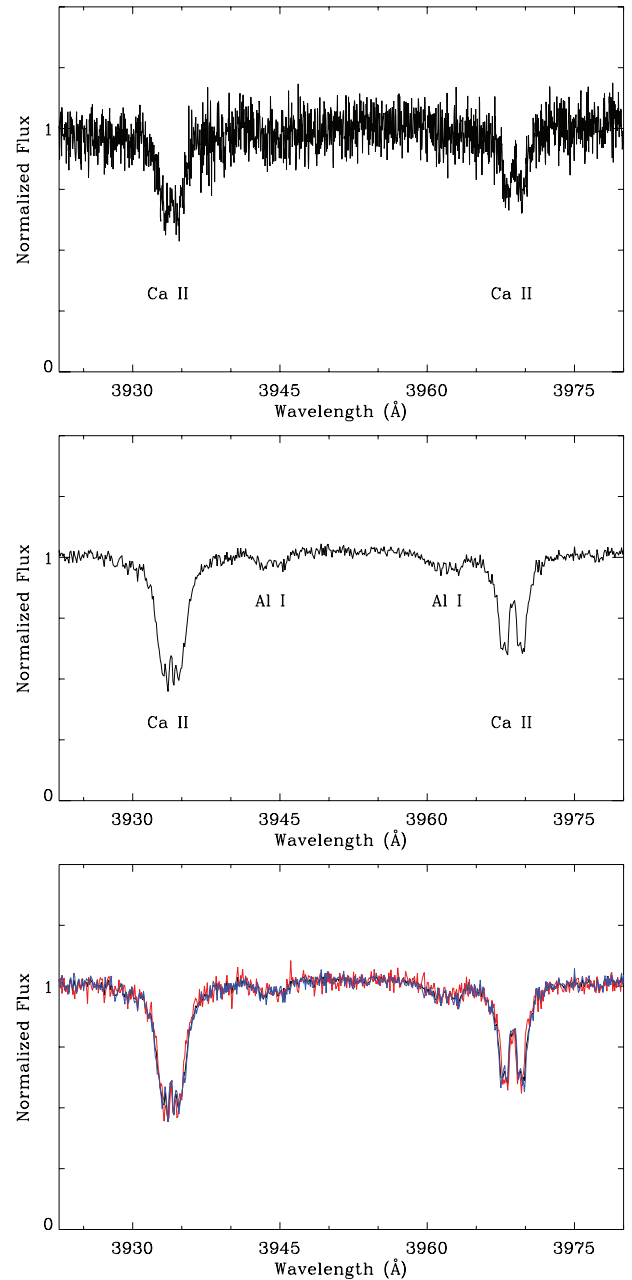
Figure 2. Upper: An example of an unbinned, single UVES spectrum of G77−50 in the Ca II H and K region. Each individual exposure exhibits these double-peaked, metal absorption lines. Middle: The same region in the combined spectrum of all 26 UVES exposures. In this deep spectrum, broad absorption features due to Al I are revealed. Lower: In red and blue, the two co-added spectral subsets discussed in Section 3.1.1 are shown, plotted on top of the master spectrum in black.

tained with these stellar parameters (listed in Table 3), together with ultraviolet through mid-infrared photometry obtained from both the ground and space. The consistency of the *Spitzer* data with the predicted stellar flux indicates excellent agreement with the model, which was fitted only at shorter wavelengths.

The co-added spectrum of G77−50 indicates the presence of several elements as well as a magnetic field. From the splitting of the various atomic lines, $B \sim 120$ kG is estimated. Such a field is too weak to have an important effect on the thermodynamic structure of the star, and the absorption features are not strong enough to effect

Table 2. Ca II H and K line velocity measurements for G77-50.

HJD−2 400 000 (d)[a]	V_- (km s^{-1})	V_+ (km s^{-1})	Instrument
51 158.874 75	−43.79 ± 1.45	+82.10 ± 1.83	HIRES
51 404.109 02	−51.36 ± 3.11	+99.77 ± 3.61	HIRES
51 737.932 10	−61.34 ± 5.43	+94.93 ± 6.89	UVES
51 740.883 65	−50.32 ± 4.75	+87.94 ± 3.73	UVES
54 743.714 92	−43.26 ± 2.69	+98.32 ± 2.32	UVES
54 743.725 96	−48.18 ± 2.71	+92.99 ± 2.21	UVES
54 743.737 82	−46.78 ± 2.78	+96.59 ± 3.60	UVES
54 743.748 87	−48.55 ± 2.61	+91.46 ± 3.16	UVES
54 743.810 40	−50.28 ± 2.87	+91.03 ± 2.64	UVES
54 743.821 49	−49.51 ± 2.15	+86.41 ± 2.90	UVES
54 744.733 66	−50.01 ± 1.79	+89.36 ± 1.82	UVES
54 744.744 71	−47.93 ± 2.43	+91.32 ± 2.41	UVES
54 744.835 45	−51.48 ± 1.99	+89.90 ± 2.40	UVES
54 744.846 56	−45.99 ± 2.04	+87.58 ± 1.80	UVES
54 747.695 94	−54.15 ± 2.32	+97.44 ± 2.32	UVES
54 747.707 00	−56.27 ± 2.51	+94.08 ± 2.27	UVES
54 749.655 00	−54.65 ± 4.22	+88.54 ± 2.95	UVES
54 749.666 05	−53.95 ± 2.97	+93.02 ± 2.77	UVES
54 750.662 19	−58.50 ± 1.87	+91.74 ± 1.96	UVES
54 750.673 21	−52.67 ± 2.09	+92.08 ± 2.26	UVES
54 759.631 48	−46.90 ± 3.15	+81.53 ± 3.08	UVES
54 759.642 59	−38.68 ± 2.40	+94.38 ± 2.40	UVES
54 760.731 76	−44.87 ± 2.32	+79.17 ± 2.55	UVES
54 760.742 81	−42.05 ± 3.26	+85.12 ± 3.15	UVES
54 767.680 13	−44.27 ± 2.07	+76.15 ± 2.15	UVES
54 767.691 18	−38.95 ± 1.70	+82.10 ± 1.35	UVES
54 795.639 88	−41.59 ± 2.30	+81.30 ± 2.55	UVES
54 795.650 95	−37.12 ± 1.92	+79.29 ± 1.82	UVES

[a]Correction made after online publication 2011 April 5: column heading amended.
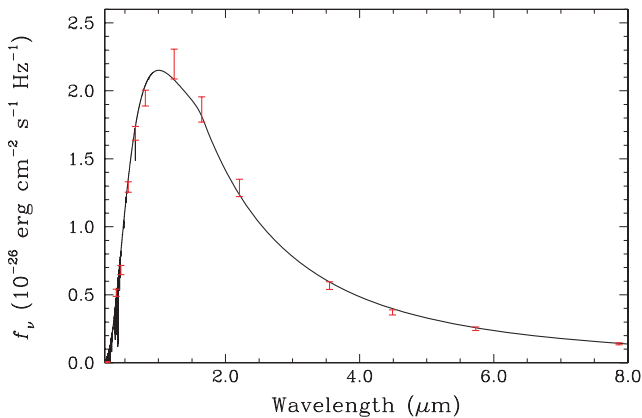
Figure 3. Spectral energy distribution of G77-50 as revealed by *GALEX* (Martin et al. 2005); *UBVRIJHK* (Bergeron et al. 1997; McCook & Sion 1999); and *Spitzer* IRAC (Farihi et al. 2008) photometry. The red error bars plot the observational data, and the black solid line is the stellar atmosphere model with parameters listed in Table 3.

the determination of the atmospheric parameters described above. This was verified explicitly *a posteriori* by comparing a pure hydrogen model energy distribution with that of a blanketed model that takes into account the presence of all the heavy elements at the derived abundances. Hence, it is safe to use the above atmospheric parameters for the detailed abundance analysis presented below. It is, however, necessary to include the effect of Zeeman splitting in synthetic spectra calculations to obtain accurate heavy

element abundances. As a first-order approximation, magnetic line splitting is explicitly included in the synthetic spectrum calculation by assuming the linear Zeeman effect in a constant magnetic field of 120 kG over the surface of the star.

In the presence of a weak magnetic field, an atomic level with total angular momentum J splits into $2J + 1$ levels with magnetic quantum number $m = -J, \ldots, +J$. For each line, all transitions were calculated between the upper and lower levels that are allowed by the selection rule ($m_u - m_l = 0, +1, -1$). Each transition is then shifted by

$$\Delta\lambda = 4.67 \times 10^{-13} \, \lambda_0^2 \, B \, (g_l m_l - g_u m_u), \tag{1}$$

where g is the Landé factor, B is the magnetic field strength in G, m is the magnetic quantum number of the level and λ_0 is the central wavelength of the line in Å. In the few cases where the Landé factor is not given in the VALD[1] line list, the term designation is used to compute the Landé factor under the L–S coupling approximation, i.e.

$$g = 1 + \frac{J(J+1) + S(S+1) - L(L+1)}{2J(J+1)}. \tag{2}$$

The relative strengths of the π, σ ($\Delta m = 0, \pm 1$, respectively) components are calculated according to Sobel'Man (1973).

For the fixed value of T_{eff} and $\log g$ determined above, a grid of synthetic, magnetic spectra is then calculated for each of the strongly detected metals, as well as for more uncertain elements. The grids typically cover an abundance range from $\log [n(Z)/n(H)] = -8.0$ to -11.0 in steps of 0.5 dex. Next, the abundance of each element is determined by fitting the various observed lines using a method similar to that described in Dufour, Bergeron & Fontaine (2005). The final adopted abundance of an element is taken as an average of all the fitted features, and these are listed in Table 4. Finally, a synthetic spectrum including all the elements is calculated with the nominal abundances and plotted over the observed spectrum in Fig. 4. In order to facilitate the line identification of the various spectral features, a non-magnetic spectrum was also calculated with the same final metal abundances.

Despite the simplicity of using a constant 120-kG field geometry for the synthetic spectrum calculations, the fits are remarkably good. Small discrepancies exist (e.g. in the wings and depth of the strong H and K lines), that are probably an indication that the field strength varies slightly over the surface. It should be noted that the master, co-added spectrum represents an average taken at various, random rotation phases. Synthetic spectrum calculations using a more realistic (dipolar) magnetic field geometry, and a suitable average over the rotation period, would probably provide a better fit to the Ca II lines, but it is unlikely that such an effort would affect the derived abundances significantly.

To find possible weak features arising from elements other than Mg, Fe, Al and Ca, a synthetic spectrum was calculated with all elements up to Ni in abundances somewhat higher than their chondritic ratios (Lodders 2003) relative to the observed Ca in G77-50. This enhanced spectrum was laid over the co-added spectrum and a careful search was done by eye, allowing identification of the strongest possible features for additional elements as well as upper limits. The search revealed the possible presence of very weak features of Mn I (4030, 4033, 4034 Å) and Cr I (4254, 4274 Å; see Fig. 4). However, the putative features are only slightly above the noise level of the spectrum and thus these elements are considered uncertain.

[1] http://vald.astro.univie.ac.at
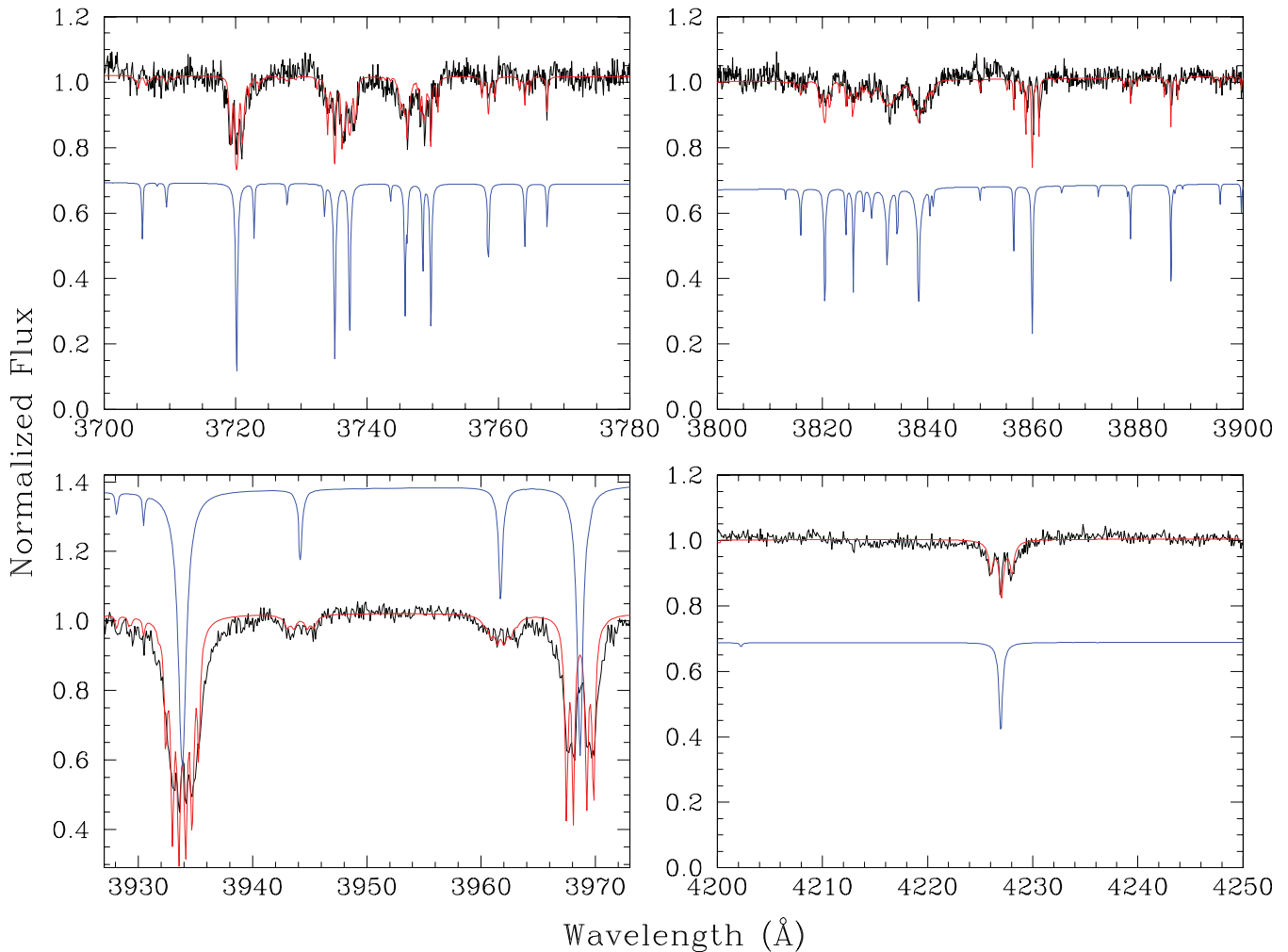
Figure 4. The combined UVES spectrum of G77-50 is shown in black and the best-fitting model in red. Vertically offset from the data, the same best-fitting, but non-magnetic model is shown in blue for line identification. The following wavelengths correspond to their non-magnetic positions. Upper left: All Fe I lines. Upper right: Fe I lines and Mg I (3832, 3838 Å). Lower left: Ca II H and K, Al I (3944, 3962 Å), and Fe I (near 3930 Å). Lower right: Ca I. Upper left: Uncertain Mn I features (4030, 4033, 4034 Å), and Fe I lines. Upper right: Uncertain Cr I features (4254, 4274 Å), and Fe I lines. Lower panels: Hydrogen Balmer lines α, β. The dashed line in the Hα panel corresponds to a model 100 K warmer than that used for the paper analysis (Section 3.3).

The Na I D doublet region also contains features (Fig. 1), but caution is warranted as this portion of the spectrum is contaminated by detector artefacts which significantly complicate the analysis. A careful examination of all the 26 individual UVES spectra indicates that the 5890-Å line is real and thus Na is likely detected in this star. Unfortunately, the energy levels involved in these transitions are too close for the linear Zeeman approximation in a 120-kG magnetic field, and the Paschen–Back regime is appropriate. Hence, the position and strength of the lines cannot be matched with the calculations presented here, and an accurate analysis of Na in this star is best left for future work with cleaner data. Nevertheless, a rough Na abundance is obtained by matching the depth of the observed feature with the Zeeman approximation model, but interpretations based on this element should be avoided.

Lastly, the synthetic Hα profile, appropriately split by a 120-kG magnetic field, is found to be slightly weaker than the observed line, whose strength depends sensitively on the effective temperature of the star. A model with a temperature increased by 100 K produces a line profile that matches the observations well (Fig. 4), and falls within the effective temperature uncertainty obtained from the fit to the photometric energy distribution.

3.3 Stellar kinematics

Armed with an average, total velocity shift of $\gamma = +20.3\,\mathrm{km\,s^{-1}}$ from the median of all the Ca II line centres in Table 2, and a mass–radius constrained by trigonometric parallax, the stellar radial velocity of G77-50 can be disentangled from its gravitational redshift. The approximation

$$z_{\mathrm{g}} \approx \frac{GM}{c^2 R} \tag{3}$$

is valid for white dwarfs. For a star of $0.60\,\mathrm{M_\odot}$ and $\log g = 8.05$, the radius is $R = 0.0121\,\mathrm{R_\odot}$ and $v_{\mathrm{g}} = 31.5\,\mathrm{km\,s^{-1}}$. Thus the radial velocity of the binary system is $v_{\mathrm{rad}} = \gamma - v_{\mathrm{g}} = -11.2\,\mathrm{km\,s^{-1}}$. Table 3 lists the resulting three-dimensional space motion for G77-50 incorporating the above radial velocity and its observed proper motion (Zacharias et al. 2010). While the velocities are not extreme, the V component lags behind the rotation of the Galaxy by $60\,\mathrm{km\,s^{-1}}$, indicating that the white dwarf belongs to the old thin or thick disc population (Pauli et al. 2006).

A total age for the white dwarf can be estimated in the following way. Taking the average and standard deviation of three independent initial-to-final mass relations (Dobbie et al. 2006; Kalirai et al. 2008;
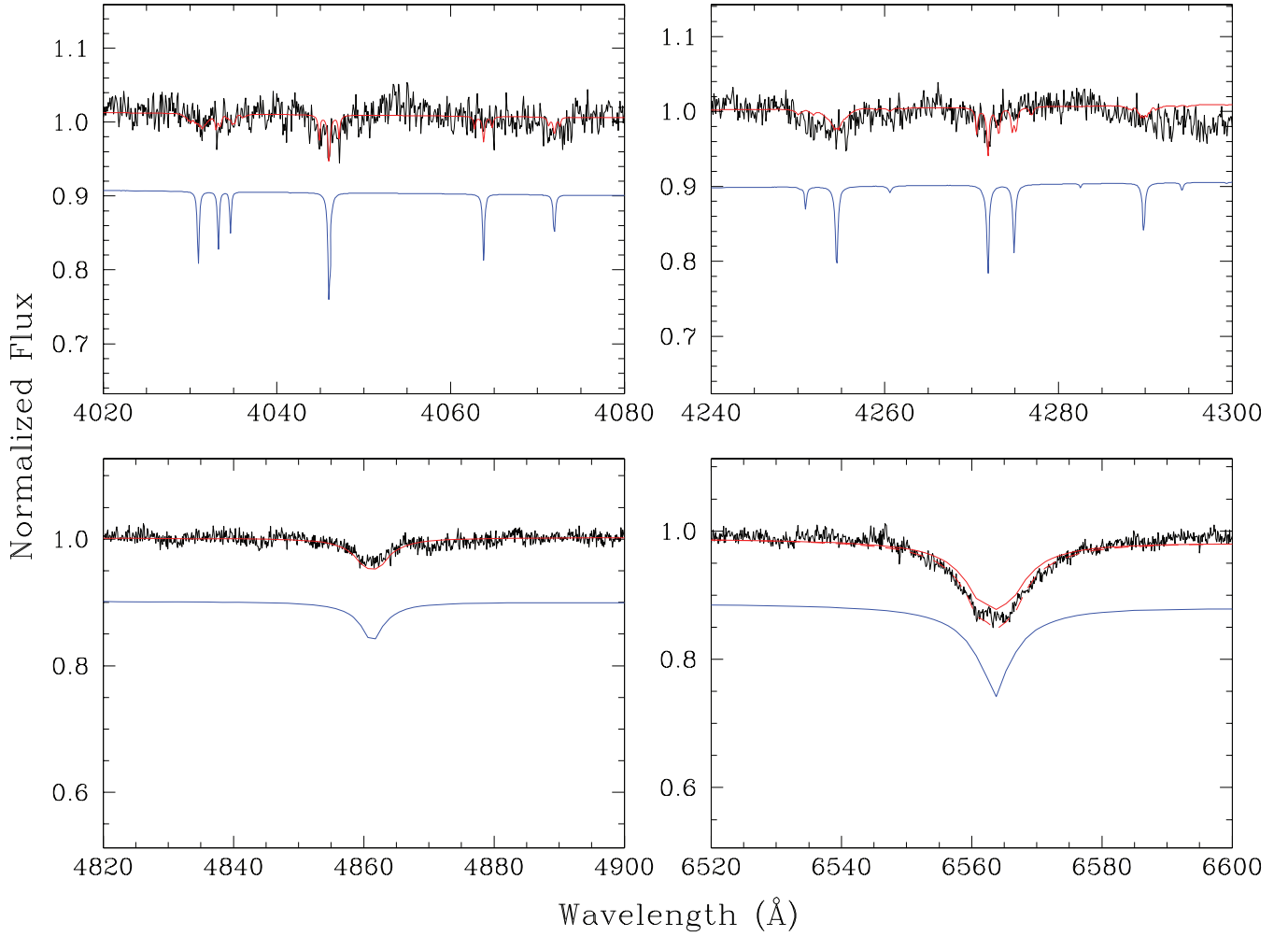
Figure 4 – *continued*

Table 3. Stellar and kinematical parameters of G77-50.

T_{eff}	5310 ± 100 K
$\log g(\mathrm{cm\,s^{-2}})$	8.05 ± 0.01
M	$0.60 \pm 0.01\,\mathrm{M_\odot}$
M_{ms}	$1.4 \pm 0.2\,\mathrm{M_\odot}$
t_{cool}	5.2 ± 0.1 Gyr
t_{ms}	3.4 ± 1.3 Gyr
t_{tot}	8.6 ± 1.3 Gyr
π_{trig}	58.02 ± 0.44 mas
(μ_α, μ_δ)	$(241, -877)$ mas yr^{-1}
$z_g\,c$	31.5 km s^{-1}
v_{rad}	-11.2 km s^{-1}
v_{tan}	74.3 km s^{-1}
v	75.1 km s^{-1}
(U, V, W)	$(-44.2, -60.5, -5.0)$ km s^{-1}

Table 4. Metal abundances and masses in G77-50.

Element	$\log[n(\mathrm{Z})/n(\mathrm{H})]$	M_z $(10^{20}$ g$)$	t_{diff} $(10^5$ yr$)$
Na[†]	-9.1	0.25	3.76
Mg	-8.3	1.62	3.85
Al	-9.2	0.20	3.72
Ca	-9.8	0.08	2.78
Cr[‡]	-9.9	0.08	2.49
Mn[‡]	-10.3	0.03	2.36
Fe	-8.7	1.31	2.33
Total	-8.0	3.57	

[†]Abundance uncertain.
[‡]Presence of this element is uncertain.
Note. Errors are 0.2 dex.

Williams, Bolte & Koester 2009), the main-sequence progenitor of G77-50 had a likely mass of $1.4 \pm 0.2\,\mathrm{M_\odot}$. The main-sequence lifetimes for stars in this mass range are obtained from the analytical formulae of Hurley, Pols & Tout (2000), and added to the cooling age of the white dwarf. This results in a total system age of $8.6 \pm$

1.3 Gyr for G77-50, a range consistent with thick disc membership, although not conclusively.

4 ORIGIN OF METALS AND MAGNETISM

Some of the material presented in this section are necessarily speculative, and are the first attempts to understand how a star such as

G77-50 came to possess its somewhat unusual characteristics. It should be the case that near-future theoretical and empirical investigations will be able to test these ideas more rigorously.

4.1 Nature of the photospheric metals

Metal diffusion time-scales and convection zone parameters for G77-50 were calculated using a complete model atmosphere with the parameters and heavy element abundances from the preceding analysis in the outer layers. This was continued to the bottom of the convection zone using pure hydrogen (Koester 2009). Table 4 lists the relevant lifetimes for all the metals detected or suspected in G77-50. The total mass of the mixing layers in G77-50 is found to be 1.23×10^{27} g, and can be combined with the photospheric abundances to obtain the current mass of each heavy element within the star. As the metals continuously sink, these calculations yield the *minimum* mass of each accreted metal, and are listed in Table 4. The total mass of metals residing in the star is 3.57×10^{20} g and equivalent to that contained in a 65-km diameter body of density $2.5 \, \mathrm{g \, cm^{-3}}$; this is the highest mass of heavy elements yet inferred within a hydrogen-rich white dwarf.

Owing to its very cool effective temperature, G77-50 possesses a sizable convection zone on par with those intrinsic to helium-rich white dwarfs (Koester 2009). Thus, the star has a commensurately long diffusion time-scale for heavy elements; e.g. 280 000 yr for Ca. In this and other respects, G77-50 is characteristic of the coolest metal-rich white dwarfs. It has modest metal abundances, with log [n (Z)/n(H)] < −8.5 for all but Mg, a relatively low time-averaged accretion rate of $3.7 \times 10^7 \, \mathrm{g \, s^{-1}}$ for all clearly detected and suspected heavy elements, and a lack of infrared excess as measured with *Spitzer* IRAC photometry (Farihi, Zuckerman & Becklin 2008; Farihi, Jura & Zuckerman 2009), indicating a dearth or absence of dust in its immediate circumstellar environment.

The relatively old white dwarf has a total space velocity of $75 \, \mathrm{km \, s^{-1}}$ and its current location is 17.2 pc from the Sun. At this speed, the star travels nearly $77 \, \mathrm{pc \, Myr^{-1}}$ and may be passing through the relatively interstellar matter-deficient local bubble (Welsh et al. 1999; Redfield & Linsky 2008), its metal content decaying from a past event within a dense region of gas and dust. Within a period just over 1 Myr, G77-50 could have been outside the local bubble, and its metal abundances would have decayed by a factor of between 20 and 100, depending on the element. With roughly 2×10^{22} g of atmospheric metals in this picture, how dense an interstellar region is necessary to account for the accretion in such a manner? For interstellar heavy elements typically contained in dust particles, the accretion rate on to a star is (Farihi et al. 2010a)

$$\dot{M}_z = \frac{\pi G M R \rho_\infty}{s} \left(\frac{T_{\mathrm{eff}}}{T_{\mathrm{ev}}} \right)^2, \tag{4}$$

where M and R are the stellar mass and radius, $s = \sqrt{v^2 + c_s{}^2}$ is the space velocity v in the supersonic regime ($v \gg c_s$) appropriate for G77-50, and T_{ev} is the evaporation temperature of the dust grains. Conservatively estimating that dust evaporates at 1000 K, the minimum density required to deposit 2×10^{22} g of metals in the star over a typical sinking time-scale of $3 \times 10^5 \, \mathrm{yr}$ is $1600 \, \mathrm{cm^{-3}}$. While such densities exist in molecular clouds, the space velocity of G77-50 requires continuous accretion over a distance of 30 pc in order that sufficient material is captured. This scenario is unlikely; one of the nearest and largest cloud complexes, the Orion nebula, is only about 8 pc in diameter.

Alternatively, the metals in the star were accreted from its circumstellar environment and were originally contained within remnant

Table 5. Metal ratios in G77-50 and other polluted white dwarfs with Al.

Star	Name	Mg/Fe	Al/Fe	Ca/Fe	Disc?
0322−019	G77-50	2.9	0.31	0.08	−
		1.2[†]	0.14[†]	0.06[†]	
	Solar	1.2	0.10	0.07	−
0208+096	G74-7	1.0	0.08	0.11	−
0300−013	GD 40	1.7	0.21	0.40	+
1633+433	G180-63	2.1	0.14	0.18	−
1729+371	GD 362	0.5	0.18	0.26	+

[†]At the end of an *assumed* accretion event 0.5 Myr prior.
Note. The three middle columns list the relative number abundances. Metal ratios for other white dwarfs with Al detections are taken from the literature (Lodders 2003; Zuckerman et al. 2003, 2007; Klein et al. 2010).

planetary bodies rich in heavy elements. The detection of both Al and Ca in the star supports a scenario in which the metals originated in a refractory-rich source such as a rocky, minor or major planet. This possibility is likely based on the weight of evidence favouring circumstellar accretion among the observed population of single, cool and metal-enriched white dwarfs (Farihi et al. 2010a; Zuckerman et al. 2010). In this scenario, the photospheric metals in G77-50 were delivered by one or more rocky planetary bodies passing close enough to the white dwarf to become tidally destroyed or otherwise accreted (Jura 2003).

For a prior pollution event, the current metal-to-metal ratios have been altered from the accreted values, via the individual heavy element sinking time-scales. Table 5 lists the photospheric abundance ratios, relative to Fe, for the four heavy elements confidently identified in G77-50. Notably, both Mg/Fe and Al/Fe appear enhanced relative to solar values and to the stars with circumstellar dust; precisely as expected in a declining phase because Fe sinks most rapidly. Interestingly, Ca/Fe is nearly solar, yet down by a factor of a few compared with the stars currently accreting from discs. Under the questionable assumption that the accreted abundances were close to solar, then the photospheric pollution halted roughly 0.5 Myr ago. In all likelihood, the accretion epoch for G77-50 ended within the last few to several diffusion time-scales, no longer than a few Myr ago. Events older than 3 Myr imply an Fe-dominated ($M_{\mathrm{Fe}}/M_z \geq 94$ per cent) parent body more massive than Pluto.

4.2 A late instability near 5 Gyr

Again, G77-50 epitomizes the older and cooler, $T_{\mathrm{eff}} < 9000 \, \mathrm{K}$ metal-rich white dwarfs: something weighty has occurred recently in these Gyr-old, presumably stable systems. Generally, the time-scale for a planetary system to dynamically settle – pre- or post-main sequence – should be 100 Myr (Debes & Sigurdsson 2002), and thus a catastrophic event at Gyr epochs is not expected for G77-50 and similar white dwarfs. Dual planet interactions will occur during this short period, if they occur at all, but instabilities among three (or more) planets may occur on longer time-scales, as hypothesized for the period of Late Heavy Bombardment in the Solar system (Gomes et al. 2005).

Following Debes & Sigurdsson (2002) and Chambers, Wetherill & Boss (1996) for the simple case of three $0.001 \, \mathrm{M_\odot}$ planets, one can calculate system architectures that give rise to an instability time-scale of 5.2 Gyr during the white dwarf evolutionary stage. Taking initial and final stellar masses to be 1.8 and $0.6 \, \mathrm{M_\odot}$ produces an (adiabatic) orbital expansion factor of 3 between the main and post-main-sequence phases. For an innermost planet now

located at 10 au, the outer planets would be near 30 and 157 au, with original – and presumably metastable – semimajor axes of 3.3, 10 and 52 au (Debes & Sigurdsson 2002). In general, for all layouts that keep the innermost planet safely outside the stellar photosphere ($a_1 > 2$ au) during the asymptotic giant branch, the planets must be spaced such that $a_2/a_1 \gtrsim 3$ and $a_3/a_2 \gtrsim 10$. Thus, the onset of instability at Gyr time-scales requires a somewhat finely tuned, increasingly wide planet spacing.

An alternative way in which an old and stable planetary system might be efficiently agitated is a stellar encounter. Though rare, at the cooling age and space velocity of G77-50, it can be shown that at least one fly-by is consistent with theoretical expectations. Dynamically, the number of stellar encounters per unit time, within a distance D of a star is given by (García-Sánchez et al. 1999)

$$N = \pi D^2 v_* \rho_*, \qquad (5)$$

where v_* is the space velocity of the white dwarf relative to passing stars and ρ_* is the local density of stars and stellar systems. From *Hipparcos* data, the velocity dispersion of stars within 2 kpc of the Sun and $|b| > 30°$ varies between 22 and 44 km s^{-1} depending on spectral type (Mignard 2000). Later-type stars tend to be kinematically more stirred as they represent, on the whole, relatively older populations. And because the most abundant stars in the Galaxy are K and M dwarfs, these relatively fast moving stars are the objects for which encounters are most likely. Taking 40 km s^{-1} for a typical field star and the 75 km s^{-1} space velocity of G77-50 yields $v_* = 85$ km s^{-1}. The local space density of stars is 0.081 pc^{-3} (T. Henry, private communication; Henry et al. 2006),[2] and equation (5) gives $N = 22$ Myr^{-1} for encounters within 1 pc. For close fly-bys that might significantly impact the outer regions of a planetary system, take $D \leq 1000$ au and then $N = 0.5$ Gyr^{-1}. If correct, and such an encounter is 50 per cent probable within each 0.5 Gyr window, then it is 99.9 per cent likely that G77-50 has suffered at least one such stellar encounter within its 5.2 Gyr cooling history.

An encounter could disturb a Kuiper Belt analogue originally orbiting at a few to several tens of au, but now residing at 1 to a few hundred au owing to mass lost during the post-main sequence. Large objects such as Sedna, whose mass is similar to Ceres, can readily be perturbed into high-eccentricity orbits by a stellar encounter, thus sending outer planetesimals towards the inner system (Kenyon & Bromley 2004). While chances are tiny that any single, distant body could be flung directly within the tidal disruption radius of the white dwarf, the perturbation of many bodies (i.e. a significant fraction of a surviving population) could result in their capture and further scattering within the inner system (Debes & Sigurdsson 2002).

A potential hurdle for this hypothesis is the total available mass that survives heating during the giant phases at these orbital distances. Out to roughly 100 au, objects composed of pure water ice and up to 100 km in diameter should sublimate completely (Stern, Shull & Brandt 1990; Jura 2004), but the overall effect on realistic bodies of heterogeneous chemical composition is unknown. For example, some models predict that subsurface volatiles should be protected by superior layers of non-volatile material such as silicates (Jura & Xu 2010). Studies of Kuiper Belt analogues in the post-main sequence may reveal the overall impact of sublimation and constrain the total mass that survives to the white dwarf stage (Bonsor & Wyatt 2010).

In contrast, Oort cloud analogues will not be destroyed via heating but are prone to dynamical evaporation in the post-main sequence if the stellar mass-loss is asymmetric (Parriott & Alcock 1998). At tens of thousands of au, stellar encounters can be frequent over Gyr time-scales typical of very cool white dwarfs such as G77-50. These events should strip away some portion of any Oort-like cloud, but also perturb another fraction on to eccentric orbits overlapping with the inner system. If such cold, outer planetesimal belts are ultimately responsible for some fraction of metal-polluted white dwarfs, then a large deposition of volatile elements would be expected, but has not yet been observed (Jura 2006; Zuckerman et al. 2007).

The subset of older and cooler metal-rich white dwarfs that G77-50 represents are a relatively high velocity group of stars, typically with $T > 50$ km s^{-1} (Aannestad et al. 1993), and the above exercise can be broadly applied to Gyr-age white dwarfs with metals. Thus, stellar encounters have the potential to make ancient planetary systems dynamically young for a brief period, and may account for the population of very cool DAZ and DZ stars, of which vMa 2 is the prototype.

4.3 Weak magnetism

In the favoured model for cool, metal-rich white dwarfs, a planetary system has survived post-main-sequence evolution (Debes & Sigurdsson 2002). Instabilities drive rocky planetary bodies such as asteroids into close approach with the compact star, where they become tidally or otherwise destroyed and are sometimes observed as dust discs (Jura 2003). For the high-eccentricity orbits necessary for the (eventual) delivery of metals on to the surface of the star, conventional-sized planets are the most efficient perturbers. In this picture, an otherwise-replete planetary system persists at metal-enriched white dwarfs, likely truncated near the maximum radius of the asymptotic giant progenitor star.

Based on precision radial velocity planet searches, 10.5 per cent of FGK dwarfs with masses in the range of 0.7–1.3 M$_\odot$ host gas giant planets within 3 au (Cumming et al. 2008). Due to the finite time period over which these searches have been carried out, most of these giant planets orbit within 1 au, and a decent fraction orbit close to their host star (the so-called hot jupiters). Relative to these findings for solar-type stars, giant planets are found more frequently, and with a higher mass distribution, in radial velocity searches of intermediate-mass stars. Both Lovis & Mayor (2007) and Johnson et al. (2007) find that planet frequency and planet (minimum) mass scale with stellar host mass, and that the fraction of gas giants orbiting within 3 au of stars with masses between around 1.5 and 2.0 M$_\odot$ is closer to 25 per cent (Bowler et al. 2010). Interestingly, stars with higher masses do not host closely orbiting giant planets, possibly due to halted orbital migration from rapid inner disc dissipation (Currie 2009), or planet–star gravitational tides (Hansen 2010).

The bulk of giant planets orbiting within a few au of their host stars will be destroyed during the post-main-sequence phases of their host stars. During the first ascent giant branch (RGB), stars with main-sequence masses above 1.0 M$_\odot$ expand to around 10–20 R$_\odot$, or 0.05–0.10 au, sufficient to swallow only the hot planets (Villaver & Livio 2009; Bowler et al. 2010). Depending on which initial-to-final mass relation one uses, the main-sequence progenitor of G77-50 was an early to late F star with a mass between 1.2 and 1.6 M$_\odot$. For an $M > 1.3$ M$_\odot$ progenitor, there is a 25 per cent chance it hosted a giant planet within a few au, but not a hot planet. In this case, the inner planet would survive the RGB intact but most likely become enveloped during the asymptotic giant branch (AGB),

---

either directly or via tidal forces; a $1.5\,M_\odot$ star has a maximum AGB radius near 2.4 au (Villaver & Livio 2007).

Depending on the mass and angular momentum of an engulfed planet, a common envelope may develop for a time sufficient to generate a magnetic dynamo (Regős & Tout 1995; Siess & Livio 1999b; Tout et al. 2008; Nordhaus et al. 2010). The eventual accretion of the planet on to the stellar core may also result in enhanced mass-loss from the giant (Siess & Livio 1999a), producing a white dwarf remnant potentially less massive than predicted by initial-to-final mass relations. If this occurs at the level of $0.05\,M_\odot$ in the white dwarf, then the inferred mass of the progenitor star will be biased towards lower, main-sequence masses. In the model of Potter & Tout (2010), the longer the common envelope environment, the larger the magnetic field strength in the resulting white dwarf plus companion merger. This model predicts fields up to 10^7 G in a common envelope lasting roughly 10^4 yr, but with a stellar companion generating the convective motions. Following Potter & Tout (2010) but reducing the companion mass by a factor of 100 (to $10\,M_J$), all else being equal, a magnetic field of 10^5 G is predicted. Interestingly, the surface field of G77-50 is 1.2×10^5 G.

4.4 Possible planetary system architecture

In the admittedly speculative picture outlined above, the primordial G77-50 system formed a gas giant that migrated through a disc to an inner orbit. Subsequently and beyond this orbit, additional planets may have formed (Mandell, Raymond & Sigurdsson 2007). As in the Solar system and a significant fraction of main-sequence stars (Su et al. 2006; Carpenter et al. 2009), a Kuiper belt analogue existed at G77-50, consisting of primordial icy and rocky bodies condensed from the stellar nebula. During the post-main-sequence evolution, the volatile outer layers of these planetesimals were lost by evaporation and radiation pressure, leaving behind objects with non-volatile surfaces and intact cores (Bonsor & Wyatt 2010; Jura & Xu 2010).

In order that a stellar encounter repopulate the inner, circumstellar regions around any star, sizable planets must exist there to trap or further scatter injected bodies. Such captured planetesimals are vulnerable to perturbations via newly established resonances on 100 Myr time-scales (Debes & Sigurdsson 2002). From this point forward in time, the eventual pollution of the star by a tidally destroyed planetesimal proceeds as envisioned for metal-rich white dwarfs with cooling ages less than 0.5 Gyr (Jura 2003; Farihi et al. 2009). If the stellar encounter hypothesis applies to G77-50 and other very cool, polluted white dwarfs, then the atmospheric metals may be a reflection of the rocky remains of primitive, outer system planetesimals rather than Solar system asteroid analogues. As such, they would have a composition distinct from objects that formed at higher temperatures in the inner system, presumably including a higher concentration of volatile elements.

Testing this hypothesis may be difficult. While cooler white dwarfs have lower atmospheric opacities and hence detection of their heavy elements is less challenging, there are two complications. The main difficulty is that the coolest DAZ and DZ stars are not amenable to ultraviolet spectroscopy, which is the ideal region to search for volatiles (or any element) in low abundance. For example, trace amounts of atmospheric carbon are only seen in the optical spectra of cool, helium-rich white dwarfs, and only at abundances $\log\,[n(\mathrm{C})/n(\mathrm{He})] > -7$ (Dufour et al. 2005). If $\mathrm{C/Fe} = 8.3$ in G77-50 as in chondrites, then it would have $\log\,[n(\mathrm{C})/n(\mathrm{H})] = -7.8$ and be undetectable in this manner. Also, it is not clear what

fraction of volatile material would remain after heating and ablation during the post-main sequence (Jura 2006).

An additional complication is that it is difficult to constrain the epoch of accretion in these cooler, metal-polluted stars. Observationally, it is rare that cool DAZ or DZ have dust discs, and this may be the result of a significant reduction in the ratio of disc lifetime to cooling age. The observed abundances can be used to constrain the epoch of accretion, but this is fundamentally biased towards the composition of Solar system objects and may not accurately reflect those of extrasolar planetary bodies. This latter concern may be partially alleviated in the growing number of DZ stars being found in the Sloan Digital Sky Survey (Dufour et al. 2007); follow up of these stars will better constrain the relative frequency of discs at older, metal-enriched stars and their abundances will hopefully provide clues to the nature of the polluting bodies.

5 CONCLUSIONS

The cool white dwarf G77-50 is found to be simultaneously metal-contaminated and magnetic. A hypothesis that may account for both properties is an evolved planetary system. While highly uncertain, it is possible that G165-7 (Dufour et al. 2006) and LHS 2534 (Reid, Liebert & Schmidt 2001) acquired their magnetic fields and photospheric metals in a manner analogous to G77-50. In this tentative picture, an inner giant planet was swallowed by the post-main-sequence progenitor, creating a common envelope whose convective motions generated the extant magnetic field. Surviving rocky planetesimals have polluted the star with several refractory metals that are typical major constituents of asteroids and inner Solar system planets (Allègre et al. 1995). However, with a cooling age of 5.2 Gyr, it is difficult to imagine a planetary system architecture with instabilities sustained over such a period. A plausible model is a stellar encounter that perturbs outer planetesimals into the inner system, where planets scatter and trap them with a renewed dynamical potential for close approaches with the white dwarf.

The exact nature of the parent body whose metals currently pollute G77-50 will likely remain uncertain for the foreseeable future. The white dwarf has been observed over a large wavelength range with the two most powerful, high-resolution optical spectrographs currently available, and with the exception of Na, the detections and abundances here are not likely to be improved upon. Furthermore, the effective temperature of the star means that there is little flux to observe with the ultraviolet spectrographs on *HST*. G77-50 and other very cool DAZ and DZ stars will have to await more powerful long-wavelength observations with *JWST* or ALMA.

REFERENCES

Aannestad P. A., Kenyon S. J., Hammond G. L., Sion E. M., 1993, AJ, 105, 1033
Allègre C. J., Poirier J. P., Humler E., Hofmann A. W., 1995, Earth Planet. Sci. Lett., 4, 515
Bergeron P., Ruiz M. T., Leggett S. K., 1997, ApJS, 108, 339

Bonsor A., Wyatt M., 2010, MNRAS, 409, 1631

Bowler B. P. et al., 2010, ApJ, 709, 396

Carpenter J. M. et al., 2009, ApJS, 181, 197

Chambers J. E., Wetherill G. W., Boss A. P., 1996, Icarus, 119, 261

Cumming A., Butler R. P., Marcy G. W., Vogt S. S., Wright J. T., Fischer D. A., 2008, PASP, 120, 531

Currie T., 2009, ApJ, 694, L171

Debes J. H., Sigurdsson S., 2002, ApJ, 572, 556

Dekker H., D'Odorico S., Kaufer A., Delabre B., Kotzlowski H., 2000, SPIE, 4008, 534

Dobbie P. D. et al., 2006, MNRAS, 369, 383

Dufour P., Bergeron P., Fontaine G., 2005, ApJ, 627, 404

Dufour P., Bergeron P., Schmidt G. D., Liebert J., Harris H. C., Knapp G. R., Anderson Schneider D. P., 2006, ApJ, 651, 1112

Dufour P. et al., 2007, ApJ, 663, 1291

Farihi J., Zuckerman B., Becklin E. E., 2008, ApJ, 674, 431

Farihi J., Jura M., Zuckerman B., 2009, ApJ, 694, 805

Farihi J., Barstow M. A., Redfield S., Dufour P., Hambly N. C., 2010a, MNRAS, 404, 2123

Farihi J., Jura M., Lee J. E., Zuckerman B., 2010b, ApJ, 714, 1386

García-Sánchez J., Preston R. A., Jones D. L., Weissman P. R., Lestrade J. F., Latham D. W., Stefanik R. P., 1999, AJ, 117, 1042

Gianninas A., Dufour P., Bergeron P., 2004, ApJ, 617, L57

Gomes R., Levison H. F., Tsiganis K., Morbidelli A., 2005, Nat, 435, 466

Greenstein J. L., 1986, ApJ, 304, 334

Hansen B. M. S., 2010, ApJ, 723, 285

Henry T. J., Jao W.-C., Subasavage J. P., Beaulieu T. D., Ianna P. A., Costa E., Méndez R. A., 2006, AJ, 132, 2360

Hintzen P., Strittmatter P. A., 1974, ApJ, 193, L111

Hurley J. R., Pols O. R., Tout C. A., 2000, MNRAS, 315, 543

Johnson J. A., Butler R. P., Marcy G. W., Fischer D. A., Vogt S. S., Wright J. T., Peek K. M. G., 2007, ApJ, 670, 833

Jura M., 2003, ApJ, 584, L91

Jura M., 2004, ApJ, 603, 729

Jura M., 2006, ApJ, 653, 613

Jura M., Xu S., 2010, AJ, 140, 1129

Jura M., Farihi J., Zuckerman B., Becklin E. E., 2007, AJ, 133, 1927

Jura M., Farihi J., Zuckerman B., 2009a, AJ, 137, 3191

Jura M., Muno M. P., Farihi J., Zuckerman B., 2009b, ApJ, 699, 1473

Kalirai J. S., Hansen B. M. S., Kelson D. D., Reitzel D. B., Rich R. M., Richer H. B., 2008, ApJ, 676, 594

Kawka A., Vennes S., 2005, in Koester D., Moehler S., eds, ASP Conf. Ser. Vol. 334, 14th European Workshop on White Dwarfs. Astron. Soc. Pac., San Francisco, p. 101

Kenyon S. J., Bromley B. C., 2004, Nat, 432, 598

Klein B., Jura M., Koester D., Zuckerman B., Melis C., 2010, ApJ, 709, 950

Koester D., 2009, A&A, 498, 517

Koester D., Rollenhagen K., Napiwotzki R., Voss B., Christlieb N., Homeier D., Reimers D., 2005, A&A, 432, 1025

Koester D., Voss B., Napiwotzki R., Christlieb N., Homeier D., Lisker T., Reimers D., Heber U., 2009, A&A, 505, 441

Lodders K., 2003, ApJ, 591, 1220

Lovis C., Mayor M., 2007, A&A, 472, 657

McCook G. P., Sion E. M., 1999, ApJS, 121, 1

Mandell A. M., Raymond S. N., Sigurdsson S., 2007, ApJ, 660, 823

Martin D. C. et al., 2005, ApJ, 619, L1

Mignard F., 2000, A&A, 354, 522

Napiwotzki R. et al., 2003, Messenger, 112, 25

Napiwotzki et al., 2004, in Hilditch R. W., Hensberge H., Pavlovski K., eds, ASP Conf. Ser. Vol. 318, Spectroscopically and Spatially Resolving the Components of the Close Binary Stars. Astron. Soc. Pac., San Francisco, p. 402

Nordhaus J., Wellons S., Spiegel D. S., Metzger B. D., Blackman E. G., 2010, Proc. Natl Acad. Sci., in press (arXiv:1010.1529)

Parriott J., Alcock C., 1998, ApJ, 501, 357

Pauli E. M., Napiwotzki R., Heber U., Altmann M., Odenkirchen M., 2006, A&A, 447, 173

Potter A. T., Tout C. A., 2010, MNRAS, 402, 1072

Reach W. T., Kuchner M. J., von Hippel T., Burrows A., Mulally F., Kilic M., Winget D. E., 2005, ApJ, 635, L161

Redfield S., Linsky J. L., 2008, ApJ, 673, 283

Regős E., Tout C. A., 1995, MNRAS, 273, 146

Reid I. N., Liebert J., Schmidt G. D., 2001, ApJ, 550, L61

Siess L., Livio M., 1999a, MNRAS, 304, 925

Siess L., Livio M., 1999b, MNRAS, 308, 1133

Sion E. M., Kenyon S. J., Aannestad P. A., 1990, ApJS, 72, 707

Smart R. L. et al., 2003, A&A, 404, 317

Sobel'Man I. I., 1973, An Introduction to the Theory of Atomic Spectra. Pergamon Press, Oxford

Stern S. A., Shull J. M., Brandt J. C., 1990, Nat, 345, 305

Su K. Y. L. et al., 2006, ApJ, 653, 675

Tout C. A., Wickramasinghe D. T., Liebert J., Ferrario L., Pringle J. E., 2008, MNRAS, 387, 897

Villaver E., Livio M., 2007, ApJ, 661, 1201

Villaver E., Livio M., 2009, ApJ, 705, L81

von Hippel T., Kuchner M. J., Kilic M., Mullally F., Reach W. T., 2007, ApJ, 662, 544

Voss B., Koester D., Napiwotzki R., Christlieb N., Reimers D., 2007, A&A, 470, 1079

Welsh B. Y., Sfeir D. M., Sirk M. M., Lallement R., 1999, A&A, 352, 308

Williams K. A., Bolte M., Koester D., 2009, ApJ, 693, 355

Zacharias N. et al., 2010, AJ, 139, 2184

Zuckerman B., Koester D., Reid I. N., Hünsch M., 2003, ApJ, 596, 477

Zuckerman B., Koester D., Melis C., Hansen B. M. S., Jura M., 2007, ApJ, 671, 872

Zuckerman B., Melis C., Klein B., Koester D., Jura M., 2010, ApJ, 722, 725

This paper has been typeset from a TEX/LATEX file prepared by the author.